**Astronomy
&
Astrophysics**

Pulsation of the K 2.5 giant star GSC 09137-03505?

Th. Kallinger[1], K. Zwintz[1], A. A. Pamyatnykh[1,2,3], D. B. Guenther[4], and W. W. Weiss[1]

[1] Department for Astronomy, University of Vienna, Türkenschanzstrasse 17, 1180 Vienna, Austria
e-mail: lastname@astro.univie.ac.at
[2] N. Copernicus Astronmical Center, Polish Academy of Science, Bartycka 18, 00-716 Warzawa, Poland
e-mail: alosza@camk.edu.pl
[3] Institute of Astronomy, Russian Academy of Sciences, Pyatnitskaya Str. 48, 109017 Moscow, Russia
[4] Institute for Computational Astrophysics, Department of Astronomy and Physics, Saint Mary's University,
Halifax NS B3H 3C3, Canada
e-mail: guenther@ap.stmarys.ca

Abstract. In July, 1999, the Hubble Space Telescope (HST) pointed for more than 8 days continuously at the globular cluster 47 Tucanae. Two guide stars were used during this campaign by the Fine Guidance Sensors (FGS). Using more than 19 million photometric FGS data for the guide star GSC 09137-03505 we found brightness variability corresponding to three approximately equidistant frequencies. The detected frequencies range from 21 to 71 μHz with amplitudes between 341 and 291 ppm. Multicolor CCD photometry was obtained at the Cerro Tololo Inter–American Observatory to derive color information for the guide stars. In addition, flux calibrated spectra were observed at the South African Astronomical Observatory. Temperature and surface gravity were determined from a comparison of observed and synthetic spectral fluxes using the NEMO (Vienna New Model Grid of Stellar Atmospheres) model atmosphere grid developed by Heiter et al. (2002, A&A, 392, 619) and Nendwich et al. (2004, CoAst, 144, 43). We also performed linear nonadiabatic analyses of various stellar models in an attempt to interprete the frequencies.

Key words. stars: evolution – stars: general – stars: individual: GSC 09137-03505 – stars: fundamental parameters – stars: oscilations – stars: low-mass, brown dwarfs

1. Introduction

Our understanding of the solar structure has been revolutionized over the last decades by the development of helioseismology which took advantage of the large number of modes detectable in the solar pulsation spectrum. Unfortunately, the inability to obtain spatial resolution for stars limits the number of detectable modes to only low degree ℓ modes. Nevertheless, detecting even just a few pulsation modes can improve substantially our knowledge about the structure of a star.

Detection of stochastically driven oscillations were reported for several giants (see Bouchy & Carrier 2003 for a review), e.g. the K0 giant star α UMa, based on star tracker data of the WIRE satellite (Buzasi et al. 2000) and for the G7 giant ξ Hya (Frandsen et al. 2002), based on radial velocity measurements with the CORALIE spectrograph. In this paper we investigate evidence for solar-type oscillations in the K2.5 giant star GSC 09137-03505 (hereafter GSC 3505).

In July, 1999, the Hubble Space Telescope (HST) pointed continuously for more than 8 days at a 4 arcmin^2 field near the core region of the globular cluster 47 Tucanae (hereafter 47 TUC) in an attempt to detect extrasolar planets far beyond our local neighborhood (Gilliland et al. 2000). During this

Table 1. Positions at Epoch 2000 (GSC-I, Lasker et al. 1990), V magnitude and spectral type (see Sect. 4 and 5) of the two guide stars used during the 47 TUC campaign.

GSC – ID	RA	Dec	m_V	Spectral type
09137 – 03505	0^{h}22^{m}51^s	−72°14′37″	12^{m}235	K 2.5 III
09137 – 02720	0^{h}23^{m}58^s	−71°54′10″	12^{m}066	K 2.5 V

campaign, the Fine Guidance Sensors (FGS) used the stars GSC 3505 and GSC 09137-02720 (hereafter GSC 2720) to control the pointing of the HST and simultaneously provide a huge amount of photometric data on the guide stars of which coordinates, V magnitudes and spectral types are listed in Table 1.

In this paper we discuss how to reduce systematic effects due to the South Atlantic Anomaly and stray light in the FGS photometry and determine the signifcance level of detected frequencies. Spectral classification and multi–color photometry allow us to estimate the fundamental parameters of GSC 3505. Finally, we try to find a pulsation model which is consistent with the found frequencies.
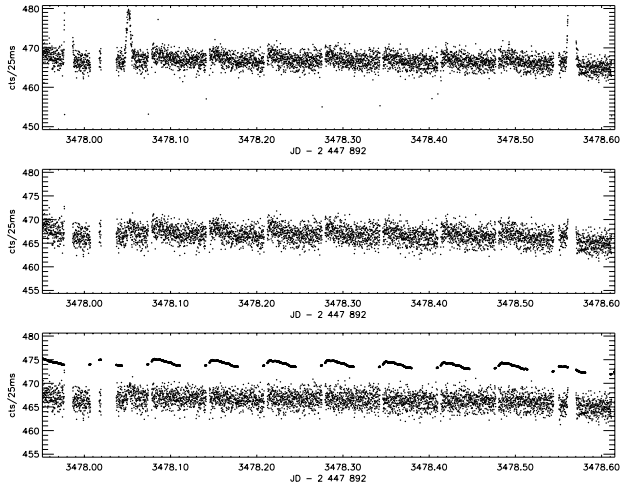
Fig. 1. Sub–set of the FGS photometry of GSC 3505 illustrating the systematically polluted data. *Top panel*: raw data, *middle panel:* after correction for the South Atlantic Anomaly (SAA), *bottom panel*: residual light curve after correcting for SAA and stray light. For a better visibility the bold line corresponding to the stray light model, which was subtracted from the data, is shifted by 7 cts/25 ms.

2. Instrument description

The Pointing Control System of the HST includes three FGSs. They are interferometry-based astrometric instruments of which at least two are used to control the tracking. Each FGS splits the light of a guide star in two orthogonaly plane polarized beams and determines, with four photomultiplier tubes, the deviation of the wavefront vector from the optical axis. Hence, while the FGSs provide the HST with the actual orientation of the satellite, they obtain 40 photon noise limited (Kuschnig et al. 1997) photometric measurements per second for all guide stars used. The more than 8 days long campaign on 47 TUC resulted in more than 19 million data points for each guide star with a duty cycle of about 67%. We average the count rates over 10 s to reduce the data volume.

3. Systematic effects

The FGS photometric data are influenced mainly by two systematic effects. The steep increase and decrease of the count rate (see, e.g., top panel of Fig. 1 at about JD 3478.05 or 3478.55) is due to the HST orbiting with a period of about 96 min. The effect is caused by particle hits inside the South Atlantic Anomaly (SAA). A less steep modulation of the count rate and with smaller amplitudes, appearing each orbit, is caused by stray light from the illuminated surface of the earth.

3.1. South Atlantic Anomaly

The SAA is characterized by a reduced magnetic field strength above the South Atlantic Ocean creating a funnel towards the ground for trapped magnetospheric protons and electrons (Skaret 1998). High energy protons impact the detectors and cause parasitic counts when the HST enters the SAA at an altitude of about 600 km. Sensitive instruments are usually switched off when passing the high intensity sections of the
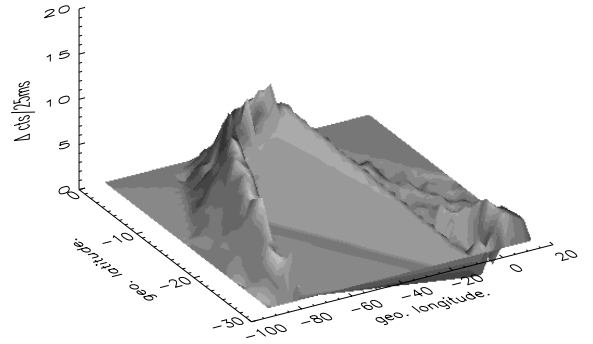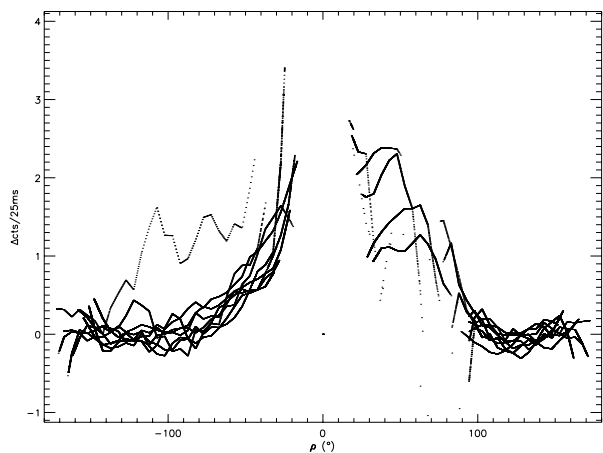

Fig. 2. Model of the photometric signal due to the SAA in the *halo* region, this is the area between the core of the SAA where the FGS were switched off and where the noise starts to increase due to high energy particles. The model corresponds to the density distribution of the trapped magnetospheric particles.

SAA, but outside the core, when the instruments start to "feel" the SAA and before they were switched off (we call this area the SAA–halo), the FGSs measure additional background signal at a rate of up to about 15 counts per 25 ms. Contrary to the approach of Zwintz et al. (1999), who removed data affected by the SAA entirely from the time series, we model the SAA and correct for the additional background flux, as is described in the following.

The raw light curve with all data points obtained outside the SAA halo is smoothed with a moving average algorithm and the gap in the light curve due to the SAA is closed by linear interpolation. This reduction step results in a reference light curve without SAA effects. The SAA halo is subdivided into $2° \times 2°$ squares in geocentric coordinates, and the median difference between the raw count rate and the reference light curve defines our SAA model for each raster element. A 2–D linear interpolation between the raster points (Fig. 2) gives the excess flux for FGS observations when the HST passes the SAA halo. The middle panel of Fig. 1 refers to a section of the lightcurve of GSC 3505 after correcting for the SAA.

3.2. Stray light due to the illuminated earth

We use the phase angle (angle between the Sun and the HST relative to the center of the earth) to characterize the stray light contribution. The HST passes the terminator at a phase angle of 90°. To estimate the stray light contribution we started from the SAA corrected light curve with all data points obtained at a phase angle larger than 100°, i.e. the HST being over the dark side of the earth and no stray light contaminating the observations. The intrinsic guide star intensity for observations at smaller phase angles is estimated by linear interpolation, thus the reference light curve is filled in for all phase angles. The stray light contribution at various phase angles can now be computed as a difference between the FGS observations and the reference light curve. To improve the statistical significance for the stray light estimate and to average over any intrinsic variations of the GS with periods different from the orbital period, we averaged the light curves obtained during 24 consecutive hours within 5° wide phase bins and smoothed the stray light

Fig. 3. Stray light contribution to the photometric signal from the illuminated earth versus phase angle ρ (angle between the Sun and the HST relative to the center of the earth). Each line corresponds to the stray light model for individual observations obtained during consecutive 24 h.
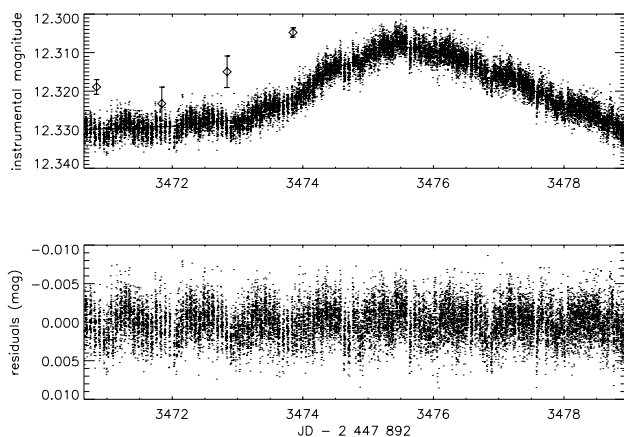
Fig. 4. The *top panel* illustrates the 30–seconds–binned light curve of GSC 3505. The nonharmonic variation with a period of about 7.5 days and a semi–amplitude of about 10 millimagnitudes is attributed to rotation. The bold line corresponds to the smooth (moving mean of 5000 data points) light curve. Diamonds represent mean Johnson–V magnitudes obtained during 4 nights at CTIO in 2001. They are shifted by about 780 days to fit the FGS light curve and offset by 0.01 mag. The *bottom panel* shows the residual light curve.

contributions plotted as a function of phase angle with a moving average. A linear interpolation between the 5° bins provides the stray light model for individual observations (Fig. 3 and bold line in the bottom panel of Fig. 1) which is applied to the SAA–corrected count rates. A subset of the resulting light curve is shown in the bottom panel of Fig. 1.

4. Frequency analysis

Data corrected for systematic effects are calibrated and dead time corrected using the photometric calibration determined by Weiss et al. (1999). The resulting light curve (top panel of Fig. 4) was analyzed with the DFT (Discrete Fourier Transformation; Deeming 1975) based Fourier analysis program with a multi–sine fit option *Period98* (Sperl 1998). It

shows a large nonharmonic variation (LNV), which probably is due to rotation, with a period of at least 7.5 days and an amplitude of about 10 millimagnitudes. Longer periods are difficult to detect with the limited time span of the observations. The period and amplitude are consistent with what was found by Edmonds & Gilliland (1996) for other K giant variables in 47 TUC.

Multicolor CCD observations of an about 7×7 arcmin large field centered on GSC 3505 were carried out with the 0.9 m telesope at Cerro Tololo Inter–American Observatory (CTIO) during 4 nights in August, 2001. The observations provide time series for 114 stars in Johnson B and V with 122 photometric measurements each. As illustrated in the top panel of Fig. 4, the CTIO data (diamonds) of GSC 3505 confirm the LNV in the FGS data if the CTIO data are shifted by 780 days. Because of a lack of standard stars in the CCD frames we were unable to transform the CTIO instrumental magnitudes to the FGS system. Hence, it is impossible to merge the data sets and improve the LNV period.

Next we investigated the residual light variations after subtracting the LNV, which was derived from smoothing the light curve (solid line in Fig. 4), with a moving average of 5000 data points (corresponding to 13.9 h). The power spectrum of this residual time series (bottom panel of Fig. 4) shows 4 significant peaks (Fig. 5). Kuschnig et al. (1997) demonstrated for comparable data that a signal-to-noise ratio (S/N) in a power spectrum of larger than 16 corresponds to a probability of more than 99.9% that a peak in the power spectrum is not produced at random (a S/N ratio of more than 13 corresponds to a probability of more than 99%). The peak f1 at $1\,\mathrm{d}^{-1}$ also appears in the Fourier spectrum of GSC 2720 which was observed simultaneously with the K giant and therefore seems to be of instrumental origin. A phase plot with this period shows a nearly sinusoidal shape indicating that higher harmonics are absent in the amplitude spectrum. The frequencies f2, f3 and f4 listed in Table 2 are approximately equidistant with an average spacing $\Delta\nu$ of about 2.16 d^{-1} (25 μHz). No comparable peaks appear in the Fourier spectrum of GSC 2720 (see bottom panel of Fig. 5). Despite a comparable brightness of the two guide stars, the noise level of GSC 3505 is clearly larger than of GSC 2720. We think that this is due to a higher activity level of the subgiant GSC 3505 compared to the main sequence star GSC 2720. In addition, more than the 3 modes might be excited in GSC 3505, but with too small amplitudes to be clearly detected.

To investigate whether these three frequencies and the spacing are an artefact, we produced 14 512 different data sets (the chosen number is random) based on the GSC 3505 observations by keeping the time marks, but randomly interchanging the magnitude values. We computed the Fourier spectrum for each set. As expected, single peaks are found with amplitudes exceeding a S/N ratio of 4 only in 18 cases (i.e. 0.12% of 14 512).

The top histogram in Fig. 6 (with $0.2\,\mathrm{d}^{-1}$ bins) illustrates how often the highest peak in an individual Fourier spectrum (independent of the S/N ratio) falls into a given frequency bin. These numbers are compared to what is expected for a uniform distribution of the peaks over all bins. The histogram shows only a marginal increase of incidence for frequency bins
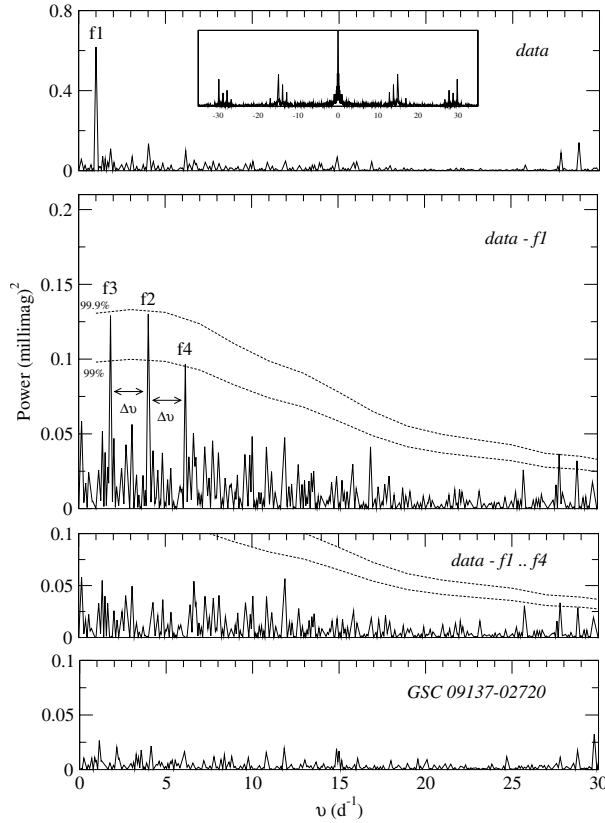
Fig. 5. The *top panel* illustrates the power spectrum for the GSC 3505 time series after subtracting a smoothed long period (rotation?) light curve. The peak *f1* at $1\,d^{-1}$ which also appears in the Fourier spectrum of the simultaneously observed guide star (GSC 2720) probably is of instrumental origin. The inserted panel shows the window function of the time series. The *second panel* shows the power spectrum after prewhitening with f1. The dotted lines correspond to significance levels described by Kuschnig et al. (1997). The peaks *f2*, *f3* and *f4* are approximately equidistant with an average spacing $\Delta \nu$ of $2.16\,d^{-1}$. The *third panel* illustrates the power spectrum after prewhitening. The *bottom panel* shows the power spectrum of GSC 2720 after prewhitening with the 1 day and the orbital periods.
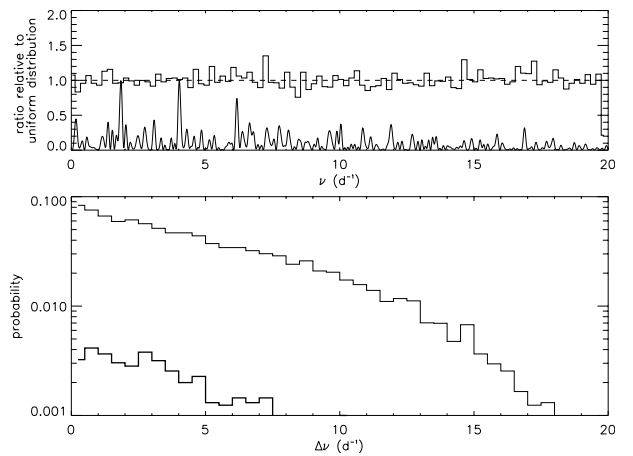
corresponding to the orbital period and half the orbital period (slightly less than 15 and $7.5\,d^{-1}$).

The histogram at the bottom of Fig. 6 shows the probability for frequencies with the two highest amplitudes (thin line) and the three highest amplitudes (thick line) being spaced by $\Delta \nu$, regardless of the *S/N*. In 41 cases (0.28 % of our 14 512 tests) we found that the spacings of 3 peaks fell into the frequency bin ranging from $2\,d^{-1} < \Delta \nu < 2.5\,d^{-1}$, but *none* of the peaks had an amplitude exceeding a *S/N* ratio of 4! Finally, the probability of finding 3 random peaks with spacings ranging from 2 to $2.5\,d^{-1}$, and where *at least one* peak has an amplitude exceeding a *S/N* ratio of 4, can be estimated to be less than 0.028%.

Concluding, we can state that it is not impossible to find a frequency triplet as described in Table 2 in *any* light curve similar to that we have obtained for GSC 3505, but it is *very* improbable.

Table 2. Oscillation frequencies detected in the photometric time series of GSC 3505 after prewhitening with f1 (see Fig. 5). The rms error in amplitude of a multi–sine fit, derived with EPSIM (Error Propagation Simulator; Reegen 2003), is given in brackets after the amplitude. The S/N is determined by dividing the amplitude by the noise in a $10\,d^{-1}$ wide bin in the residual spectrum centered on the peak. The spacings between consecutive peaks are listed in column $\Delta \nu$.

| ID	ν		$\Delta \nu$		Amplitude	S/N
	(d^{-1})	(μHz)	(d^{-1})	(μHz)	(ppm)	
f3	1.846	21.365			331($\pm$22)	4.0
f2	4.028	46.624	2.182	25.259	341($\pm$28)	4.2
f4	6.167	71.378	2.139	24.754	291($\pm$21)	3.6

Fig. 6. The *top* histogram with frequency bins of $0.2\,d^{-1}$ illustrates the incidence of the highest peaks in 14 512 different Fourier spectra ranging from 0 to $20\,d^{-1}$. These spectra were computed from time series with time marks identical to the GSC 3505 time series, but with randomly interchanged magnitude values. The numbers are normalized to a uniform distribution of highest peak frequencies. No excess is evident in the ranges of the 3 observed frequencies (for comparison the power spectrum is inserted in the histogram). The *bottom* histogram with frequency bins of $0.5\,d^{-1}$ shows the probability that the frequencies with the two highest amplitudes (thin line) and the three highest amplitudes (thick line) are spaced by $\Delta \nu$.

5. Spectral classification and fundamental parameters

For a spectral type classification we used a flux calibrated spectrum which was acquired in July 2001 with the 1.9 m telescope at the South African Astronomical Observatory. The observed spectral flux was compared with synthetic spectral fluxes from the NEMO[1] model atmosphere grid (Heiter et al. 2002; Nendwich et al. 2004) using a χ^2 test. The best fit was obtained for a model atmosphere with an effective temperature of 4400 K, a log g of 2.2 and a solar-like metallicity, which corresponds to a K 2.5 giant star (Gray 1992). A formal accuracy

---

[1] Vienna New Model Grid of Stellar Atmospheres, 2003, http://ams.astro.univie.ac.at/nemo/
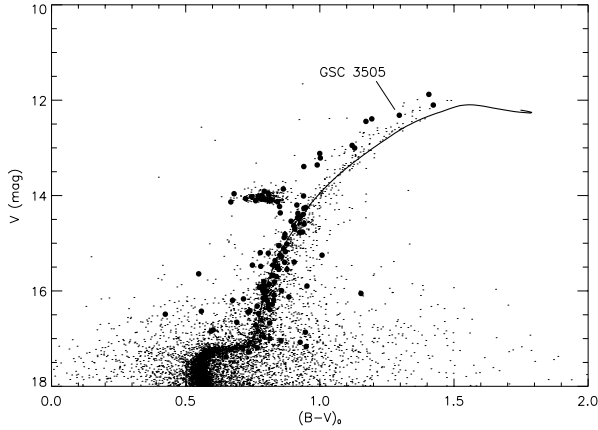
Fig. 7. Color–magnitude diagram of the 47 TUC cluster based on data (small dots) of Hesser et al. (1987) and Kaluzny et al. (1998). The CTIO data are indicated as large dots. An α–enhanced Y^2 isochrone of 11.5 Gyr, [Fe/H] = –0.76, [α/Fe] = +0.15 and $(Y, Z) = (0.238, 0.004)$ is overplotted and shifted according to a distance modulus of $13^{\mathrm{m}}5$.

of ± 100 K and ± 0.2 for $\log g$ was determined by comparing the quality of the fit to neighbouring models.

47 TUC is a well investigated globular cluster close to the Galactic disk with a distance modulus of $13^{\mathrm{m}}5$ and an age of about 11.5 Gyr (Gratton et al. 2003). In Fig. 7 we compare colors and Johnson V magnitudes of 114 stars observed during the CTIO observing run with a color–magnitude diagram based on data provided by Hesser et al. (1987) and Kaluzny et al. (1998). GSC 3505 is located on the giant branch of the cluster and has a $(B - V)_0$ color of about 1.27 mag (corresponding to 4300 K, Gray 1992) which confirms the effective temperature derived from our spectral classification.

If GSC 3505 is indeed a member of the cluster, we can estimate its mass to be about $0.9\,M_\odot$ using the α-enhanced Y^2 isochrone (Kim et al. 2002) of 11.5 Gyr, [Fe/H] = –0.76, [α/Fe] = +0.15 and $(Y, Z) = (0.238, 0.004)$. The absolute magnitude $M_V = -1.27 \pm 0.08$ can be derived from the average V magnitude of $12^{\mathrm{m}}235 \pm 0.003$ and the distance modulus for 47 TUC $(m - M)_V = 13^{\mathrm{m}}5 \pm 0.08$. The bolometric correction BC for a giant star of this temperature is –0.826 (Reed 1998; Cayrel et al. 1997) resulting in an estimated luminosity of $119 \pm 9\,L_\odot$ and a radius of $18.8 \pm 1.1\,R_\odot$ according to

$$L/L_\odot = 79.43 \times 10^{-0.4 \cdot (M_V - BC)} \tag{1}$$

$$R/R_\odot = 2.974 \times 10^8 \cdot T_{\mathrm{eff}}^{-2} \times 10^{-0.2 \cdot (M_V - BC)}. \tag{2}$$

This is again consistent with the luminosity and radius for a K 2.5 giant star (Gray 1992).

6. Discussion

A single evolutionary track for $0.9\,M_\odot$, $Y = 0.24$ and $Z = 0.005$ was constructed using the Yale stellar evolution code (YREC, Guenther et al. 1992). Note that the relative element abundances of the metals are solar so that the models do not exactly correspond to the Y^2 Isochrone models. The adiabatic frequencies of the radial p-modes were then calculated for all of
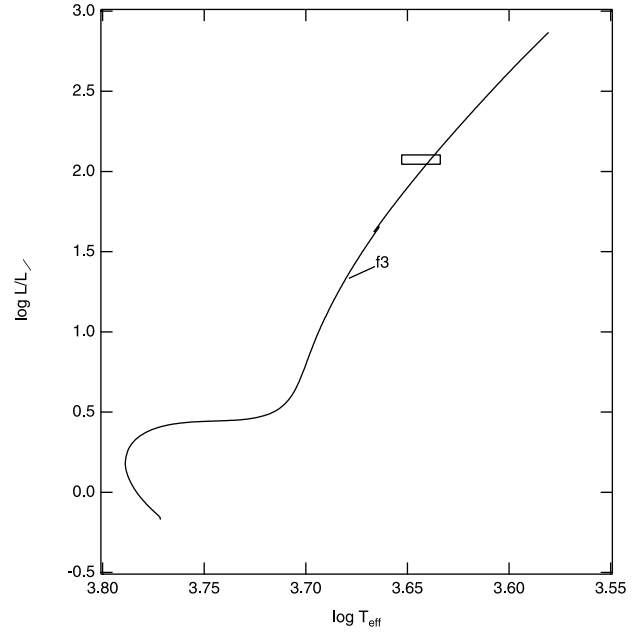

Fig. 8. HR-diagram showing the uncertainty box location of GSC 3505 and an evolutionary track corresponding to $0.9\,M_\odot$, $Y = 0.24$, $Z = 0.005$. The location along the track where the fundamental mode matches f3 is also indicated.
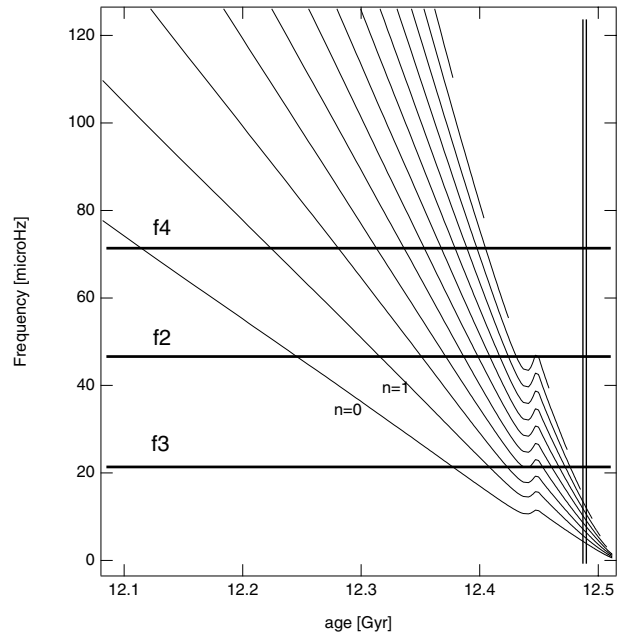
Fig. 9. The evolution of all radial p-modes from the fundamental mode to the acoustic cut-off frequency for the models just along the giant branch of the track plotted in Fig. 8 The frequencies of the three observed modes are indicated by thick horizontal lines. The two vertical lines indicate where the models lie within the uncertainty box for GSC 3505. The units for the ordinate are μHz, and the conversion factor to d^{-1} is 0.0864.
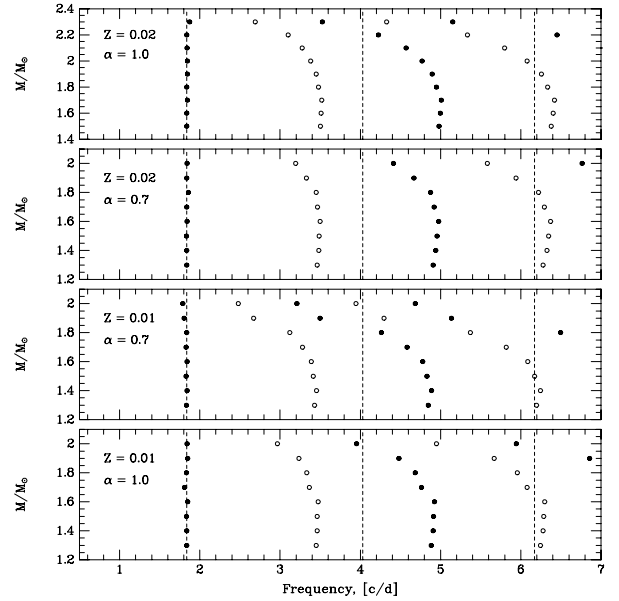
the models along the track using Guenther's oscillation code (Guenther 1994). Modes from the fundamental mode to the acoustic cut-off frequency were computed. Figure 8 shows the evolutionary track together with an error box identifying the approximate position of GSC 3505. Figure 9 shows the
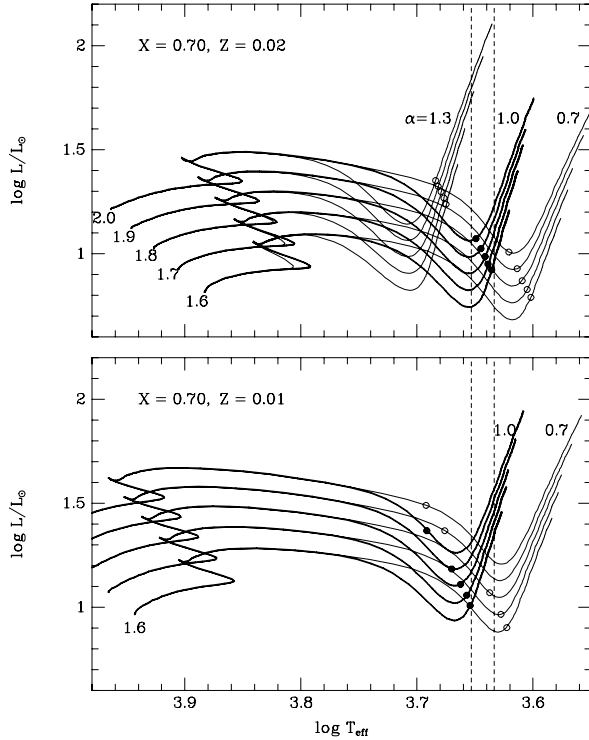
Fig. 10. Evolutionary tracks for indicated values of mass in solar units, and for mixing-length parameter α. Filled and open circles correspond to the models whose radial fundamental frequency is approximately equal to the observational frequency f3 = 1.846 d^{-1}. The upper and lower panels correspond to heavy–element abundances $Z = 0.02$ and 0.01, respectively. The vertical dashed lines mark the range of allowed effective temperatures, from 4500 to 4300 K, as obtained from the spectral classification of GSC 3505.

Fig. 11. Frequencies of radial oscillations of stellar models with different masses, heavy element abundances, Z, and mixing-length parameter α. The upper two panels show modes based on models with the solar metallicity. The dashed lines correspond to the three observed frequencies. Each set of model parameters is selected to fit the lowest detected frequency as fundamental radial mode. The filled circles indicate the fundamental radial modes, second and fourth overtones of the corresponding model, the open circles correspond to the first and third overtones.

evolution of the radial acoustic modes as a function of time for the models along the gaint branch of the track. The mode frequencies decrease in inverse proportion to the radius of the models. The uppermost frequencies plotted correspond to the acoustic cut-off frequency. We also denote with thick horizontal lines the frequencies of the f3, f2, and f4 modes. The pair of vertical lines indicates the very narrow age range where the models pass through the uncertainty box in the HR-diagram. We see immediately that the three observed modes lie above the acoustic cut-off frequency for models within the HR-diagram uncertainty box. Indeed if the lowest frequency f3 corresponds to a fundamental mode, then the location of the model is as indicated by the tag "f3" in Fig. 8. Considering that GSC 3505 is a member of 47 TUC it appears unlikely that the three observed oscillation frequencies are radial p-modes.

47 TUC is a global cluster crossing the Galactic disk. Ignoring the estimates for $\log g$, $\log L$ and age, it would not be surprising to find a background star in the same line-of-sight. We performed evolutionary computations and a linear non–adiabatic analysis of pulsation (Dziembowski 1977) of various stellar models with different masses, chemical compositions and convection parameters (for details of the method and input physics see Pamyatnykh 1999 and references therein). We studied models with effective temperatures around

the observational range from 4300 to 4500 K which are the limits determined from our spectral classification, and we fitted the radial fundamental frequency to the observed value of f3. All low-order acoustic modes are unstable in this range. However, our understanding of the excitation mechanism in these cold models with effective convection in the envelope is not satisfactory. The excitaion here is determined significantly by the interaction between pulsation and convection which is still poorly understood. We used the mixing-length formalism and simply neglected the Lagrangian variation of the convective energy flux during an oscillation cycle. The problem in relation to pulsation of red giants was discussed by Dziembowski et al. (2001).

Figure 10 illustrates the sensitivity of the models to the efficiency of convection in the stellar envelope and to the changes of the heavy–element abundance. Open and filled circles in both panels mark the models whose radial fundamental frequency is approximately equal to 1.846 d^{-1} i.e. to the observed frequency f3. For $Z = 0.02$ the fitted models with mixing-length parameter $\alpha = 1.0$ fall into the allowed range of effective temperature. These models are located at the bottom or in the middle of the red giant branch. For $Z = 0.01$ the fitted models with $\alpha = 0.7$ are slightly less evolved. Note that evolution to and on the red giant branch is quite fast, therefore evolutionary changes of periods must be large, they occur by approximately two orders of magnitude faster than period changes during the main-sequence evolution of models of the same mass. For example, for a 2 $M_\odot$ model the rate of the relative period change, $(1/P_F)dP_F/dt$, is about 12×10^{-8} year^{-1} which is comparable

with fast period changes during the pre-MS evolution near the ZAMS (see Breger & Pamyatnykh 1998).

Figure 11 shows the spacing between consecutive radial overtones of fitted models. It is clearly seen that none of the models can reproduce the observed frequencies as consecutive overtones of the radial modes. However, for $Z = 0.01$ the $2\,M_\odot$ model with $\alpha = 1.0$ and a model of the mass between 1.8 and 1.9 $M_\odot$ with $\alpha = 0.7$ approximately fit observed frequencies as every second radial mode – as fundamental mode, second and fourth overtone. In the HR-diagram, these models are in the final evolutionary stage of expansion to the red giant branch.

7. Conclusions

We have shown that the probability is very high that the observed frequency triplet is indeed intrinsic and not a product of chance. However, in a wide range of stellar model parameters we are unable to interpret the observed frequencies as consecutive radial modes. This is particularly true if GSC 3505 is a member of 47 TUC. But also if it is a less evolved background star with comparable temperature it would be difficult to understand why only every second overtone should be excited.

References

Bouchy, F., & Carrier, F. 2003, Ap&SS, 284, 21
Breger, M., & Pamyatnykh, A. A. 1998, A&A, 332, 958
Buzasi, D., Catanzarite, J., Laher, R., et al. 2000, ApJ, 532, L133
Cayrel, R., Castelli, F., Katz, D., et al. 1997, ESA SP-402, 433
Christy, R. F. 1966, ARA&A, 4, 353
Deeming, T. J. 1975, Ap&SS, 36, 137
Dziembowski, W. A. 1997, AcA, 27, 95
Dziembowski, W. A., Gough, D. O., Houdek, G., & Sienkiewicz, R. 2001, MNRAS, 328, 601
Edmonds, P. D., & Gilliland, R. L. 1996, ApJ, 464, L157
Frandsen, S., Carrier, F., Aerts, C., et al. 2002, A&A, 394, L5
Gilliland, R. L., Albrow, M. D., Brown, T. M., Charbonneau, D., & Burrows, A. 2000, AAS, 196.0202G
Gratton, R. G., Bragaglia, A., Carretta, E., et al. 2003, A&A, 408, 529
Gray, D. F. 1992, The observation and analysis of stellar photospheres (Cambridge University Press)
Guenther, D. B., Demarque, P., Kim, Y.-C., & Pinsonneault, M. H. 1992, ApJ, 387, 372
Guenther, D. B. 1994, ApJ, 442, 400
Heiter, U., Kupka, F., van 't Veer-Menneret, C., et al. 2002, A&A, 392, 619
Hesser, J. E., Harris, W. E., & Vandenberg, D. A., et al. 1987, PASP, 99, 739
Kaluzny, J., Wysocka, A., Stanek, K. Z., & Krzeminski, W. 1998, AcA, 48, 439
Kim, Y.-C., Demarque, P., Yi, S. K., & Alexand, D. R. 2002, ApJS, 143, 499
Kjeldsen, H., & Bedding, T. R. 1995, A&A, 293, 87
Kuschnig, R., Weiss, W. W., Gruber, R., Bely, P. Y., & Jenker, H. 1997, A&A, 328, 544
Lasker, B. M., Sturch, C. R., McLean, B. J., et al. 1990, AJ, 99, 2019
Nendwich, J., Nesvacil, N., Heiter, U., Kupka, F., & Weiss, W. W. 2004, CoAst, 144, 43
Pamyatnykh, A. A. 1999, Acta Astron., 49, 119
Reed, C. 1998, JRASC, 669, 36
Reegen, P. 2003, ESA SP-538, ed. S. Aigrain, & F. Favata, 389
Skaret, K. A. 1998, Space Weather and the MOST Microsatellite, Department of Physics and Astronomy, The University of British Columbia
Sperl, M. 1998, Comm. Astroseismology (Vienna), 111, 1
Weiss, W. W., Kuschnig, R., Witeschnik, A., & Zwintz, K. 1999, CoAst, 129
Zwintz, K., Kuschnig, R., Weiss, W. W., Gray, R. O., & Jenkner, H. 1999, A&A, 343, 899